MCP Papers in Press. Published on August 20, 2012 as Manuscript M112.021048

Proteomic characterization of phagosomal membrane microdomains during phagolysosome biogenesis and evolution

Guillaume Goyette[1*], Jonathan Boulais[1,7,8*], Nicholas J Carruthers[2], Christian R Landry[3,4], Isabelle Jutras[1], Sophie Duclos[1], Jean-François Dermine[1], Stephen W. Michnick[3], Sylvie LaBoissière[6], Gilles Lajoie[2], Luis Barreiro[8], Pierre Thibault[5]and Michel Desjardins[1,7]**

[1]Département de pathologie et biologie cellulaire, Université de Montréal, C.P. 6128, Succ centre ville, Montréal, Québec, H3C 3J7, Canada

[2]Department of Biochemistry, University of Western Ontario, Siebens-Drake Research Institute, London, ON, N6A 5C1, Canada

[3]Département de biochimie, Université de Montréal, C.P. 6128, Succ centre ville, Montréal, Québec, H3C 3J7, Canada

[4]Département de Biologie et Institut de Biologie Intégrative et des Systèmes (IBIS), Université Laval, Québec, G1V 0A6, Canada

[5]Institut de recherche en immunologie et cancérologie (IRIC), C.P. 6128, Succ centre ville, Montréal, Québec, H3C 3J7, Canada

[6]Proteomics Unit, McGill University and Génome Québec Innovation Centre, 740, av. Docteur Penfield, Montreal, Qc, H3A 1A4, Canada

[7]Département de microbiologie et immunologie, Université de Montréal, C.P. 6128, Succ centre ville, Montréal, Québec, H3C 3J7, Canada

[8]Département de pédiatrie, Centre de recherche de l'hôpital Sainte-Justine, Université de Montréal, Montréal, Québec, H3T 1C5, Canada

* These authors contributed equally to this work.

**Address correspondence to: Michel Desjardins, Département de pathologie et biologie cellulaire, Université de Montréal, C.P. 6128, Succ centre ville, Montréal, Québec, H3C 3J7, Canada and Pierre Thibault, Institut de recherche en immunologie et cancérologie (IRIC), C.P. 6128, Succ centre ville, Montréal, Québec, H3C 3J7, Canada.

Tel. 514 343-7250
Fax 514 343-2569
Email: michel.desjardins@umontreal.ca

Running title : **Characterization of phagosomal membrane microdomains**

Abbreviations List

DRMs, detergent resistant membranes; DSMs, detergent soluble membranes; HB, homogenization buffer; LC, Liquid chromatography; LPG, lipophosphoglycan; MS/MS, tandem mass spectrometry; PCA, Protein-fragment Complementation Assay; PNS, post nuclear supernatant; RPC, redundant peptide counts; TCL, total cell lysate; TM, total membranes.

Summary

After their formation at the cell surface, phagosomes become fully functional through a complex maturation process involving sequential interactions with various intracellular organelles. In the last decade, series of data indicated that some of the phagosome functional properties occur in specialized membrane microdomains. The molecules associated with membrane microdomains, as well as the organization of these structures during phagolysosome biogenesis are largely unknown. In this study, we combined proteomics and bioinformatics analyses to characterize the dynamic association of proteins to maturing phagosomes. Our data indicate that groups of proteins shuffle from detergent-soluble to detergent-resistant membrane microdomains during maturation, supporting a model in which the modulation of the phagosome functional properties involves an important reorganization of the phagosome proteome by the coordinated spatial segregation of proteins.

Introduction

Phagocytosis, the mechanism by which large particles are internalized, leads to the formation of phagosomes, a specialized organelle in which the engulfed material is degraded (1, 2). In mammals, various cells including macrophages, neutrophils and dendritic cells display remarkable phagocytic activities, rapidly eliminating microorganisms, foreign inert particles, and apoptotic cells. The killing of microorganisms by professional phagocytes precludes the emergence of infectious diseases. This innate immune process is followed by the degradation of microbes in a highly concentrated mixture of hydrolases, activated by the acidic pH generated in the phagosome lumen, generating antigenic peptides that are displayed at the cell surface, enabling their recognition by T lymphocytes (3). The peptides not loaded on MHC molecules are fully degraded in phagolysosomes and the end products are likely recycled from phagosomes by a variety of transporters (1). The establishment of these functional properties involves a complex remodeling of phagosomes, referred to as phagolysosome biogenesis (4, 5). This highly regulated process requires the fusion of nascent phagosomes with *trans* Golgi-derived vesicles, early endosomes, late endosomes and ultimately lysosomes (1, 2). These fusion events are believed to alter significantly the proteome of phagosomes during phagolysosome biogenesis and regulate their functional properties (6).

The capacity to kill and degrade microbes is one of the many functions that phagosomes acquire during phagolysosome biogenesis. In a previous study, we identified more than 140 proteins associated with phagosomes (7), leading to the proposal of novel mechanisms to explain phagosomal functions such as antigen cross-presentation (8). This proteomics study also shown the presence on phagosomes of proteins known to segregate into lipid rafts at the cell surface,

such as flotillin-1 and prohibitin, leading to the proposal that membrane microdomains might also assemble on phagosomes. At the plasma membrane, these structures constitute foci of specialized functions, notably for signal transduction (9). Further biochemical and morphological analyses confirmed the presence of membrane microdomains on phagosomes (10). The role of membrane microdomains and the molecular nature of these structures in phagosomes is still poorly understood. Recent data indicated that two phagosomal protein complexes, V-ATPase and NADPH oxidase may use membrane microdomains as assembly platforms (11). Furthermore, the potential involvement of phagosome microdomains in innate immunity was highlighted by the finding that at least two unrelated pathogens, the Gram-negative bacteria *Brucella* and the intracellular parasite *Leishmania donovani*, target phagosome lipid rafts as a strategy to evade host-defence mechanisms (12-14). Hence, the molecular characterization of the detergent-soluble and -insoluble fractions isolated from phagosomes should provide unique insights into the mechanisms used by pathogens to alter the functional properties of this organelle. Different approaches have been used to study membrane microdomains, including imaging techniques such as fluorescence resonance energy transfer (FRET), fluorescence photoactivation localization microscopy (FPALM), as well as cell fractionation procedures using non-ionic detergents to enrich detergent-resistant membrane domains (15). Imaging approaches highlighted the fact that cholesterol-enriched membrane microdomains are dynamic microscopic structures of less than 20 nm in range. On the other hand, detergent-based fractionation approaches have been extensively used to identify key components of membrane microdomains, including series of signaling factors (16-18). Although the exact nature and the level of correspondence of the membrane microdomains studied by the morphological and biochemical approaches is still actively debated, similar sets of proteins have been identified in these structures (15).

In the present study we used quantitative proteomics approach to characterize, for the first time, the modifications of lipid rafts proteins occurring during the biogenesis of an intracellular organelle. Our data indicate that segregation of sets of proteins in sub-regions of the phagosome membrane occurs throughout the biogenesis and maturation of phagolysosome, introducing the concept that spatiotemporal reorganization of the phagosome proteome plays a key role in the establishment of the functional properties of this organelle.

Experimental Procedures

Cell Culture and Phagosome Isolation

The murine macrophage-like cell line J774 was cultured in Dulbecco's modified Eagle's medium high glucose (Sigma) supplemented with 10% heat-inactivated foetal bovine serum, 1% glutamine, 100 units/ml penicillin, and 100 mg/ml streptomycin at 37 °C in a 5% CO_2 atmosphere. Cells were grown to 80% confluence in Petri dishes prior to each experiment. To form phagosomes, J774 macrophages were fed with 0.8 mm blue dyed latex beads (Estapor® Microsphères) diluted 1:50 in culture medium without serum. Cells were allowed to internalize beads for 15 or 30 min at 37 °C. Cells were then washed two times for 5 min at room temperature with PBS to remove non-internalized beads, and were further incubated for increasing periods of time (0 min, 30 min, 240 min) to obtain early and late phagosomes. Phagosomes were then isolated on sucrose step gradients as described previously (10), a process generating highly purified organelles as demonstrated by western blotting experiments (4, 19). Purified phagosomes were resuspended in TNE buffer (25 mM Tris, 150 mM NaCl, 5 mM EDTA), transferred to an Eppendorf tube and frozen at -20°C. Samples were identified as 30/0, 30/30 or 30/240 phagosomes, referring to the 3 time-points (pulse/chase periods) analyzed.

Isolation of phagosome microdomains

Isolated phagosomes (0.15 ml suspension of phagosomes purified from 1.4 x 10^8 cells) were equilibrated to 1% Triton X-100 on ice by adding an identical volume of TNE buffer containing 2% Triton X-100, and shaken gently 30 min at 4°C to solubilize phagosomal membranes. Latex beads were then pelleted twice by microcentrifugation (5 min at 15 000 rpm), and the final supernatant containing both the solubilized and the detergent-resistant phagosome

components brought to a final concentration of 40% Optiprep™, by adding 0.6 ml of 60% Optiprep™ stock in TNE buffer. This was poured at the bottom of an Ultraclear centrifuge tube (Beckman). Finally, 3.0 ml of 30% Optiprep™ and 0.6 ml of TNE buffer were layered on top. After 4 h of centrifugation at 40 000 rpm (SW60 rotor), to float the insoluble membranes, 7 fractions of 0.6 ml were collected from the top. Proteins were then precipitated with methanol/chloroform according to established protocols (20) and resuspended in Laemmli buffer for Western blotting.

Western and slot blotting

For Western blot analysis, an identical amount of phagosomes from each sample was used, based on the latex-bead concentration as indicated above. The protein concentration in the total cell lysate (TCL) and total membranes (TM) was evaluated using the EZQ assay (Molecular Probes) and identical amounts of protein were loaded for Western blot. The mouse anti-Flotillin-1 mAb and the mouse anti-Nicastrin IgG2a were from BD Bioscience, the rabbit anti-Rab5a polyclonal antibody was from Santa Cruz. The 1D4B rat anti-LAMP1 monoclonal antibody was from the Developmental Studies Hybrodoma Bank University of Iowa. NaK ATPase α mouse monoclonal IgG1 was from ABR Affinity BioReagents. RGS19 chicken polyclonal antibody and the Gp91phox was from ABCAM. Monoclonal antibody directed against the N-terminal peptide of human stomatin was a kind gift from Dr. R. Prohaska (21). To detect the lipid ganglioside GM1, we used slot blotting with HRP-conjugated cholera toxin subunit B from Sigma.

Sample preparation for Protein Mass Spectrometry and Data Analysis

Two fractions of the Optiprep™ gradient (Fig.1B) were processed for protein

identification by mass spectrometry. The proteins in fraction 1, which contained detergent resistant membranes (DRMs), and the proteins in fraction 7, which contained the bulk of solubilized phagosome membranes (or detergent soluble membranes; DSMs), were precipitated with methanol/chloroform, resuspended in Laemmli buffer and loaded on a NuPage 12% Bis-Tris pre-cast gel (Invitrogen) for a 3 cm migration. After a silver nitrate or a Coomassie blue staining, the resulting 3 cm gel was cut in 1mm bands irrespective of band positioning. Gel bands were subjected to reduction, alkylation and in-gel tryptic digestion in an automated MassPrep Workstation (Waters, Millford, MA) as previously described (22). All mass spectrometry analyses were performed on a QTOF Micro (Waters) equipped with a Nanosource (New Objective, Woburn, MA) modified to hold the PicoFrit column tip near the sampling cone. Mass spectrometry data were collected with the following data dependant acquisition settings: 1 second in MS mode, 1 precursor ion selected based on intensity (25 cps) and charge state (+2, +3, and +4) with a maximum collection time of 4 seconds in MS/MS acquisition mode. A total of 6 experimental conditions were analysed, namely fraction 1 (DRM) and fraction 7 (DSM) of phagosomes isolated at 3 different time-points (30/0, 30/30 and 30/240). For each condition, samples generated from 3 independent experiments were analyzed in the mass spec (n=3).

MS/MS raw data were transferred from the QTOF Micro computer to a 50 terabytes server and automatically manipulated for generation of peak lists by employing Distiller version 2.0.0 (http://www.matrixscience.com/distiller.htmls) software with peak picking parameters set at 30 for Signal Noise Ratio and at 0.6 for Correlation Threshold. This reduced noise and produced a list of distinct peptide peaks in which all members of the isotopic clusters were collapsed into an equivalent monoisotopic peak. The peak list data was then searched against the Universal Protein Resource (UniProt) (http://www.pir.uniprot.org/) database (*Mus musculus* - March 2012

release) containing 76 940 protein sequences by using Mascot (http://www.matrixscience.com) version 2.1.04, and restricting the search to a maximum of 1 missed (trypsin) cleavage, fixed carbamidomethyl alkylation of cysteines, variable oxidation of methionine, ±0.5 mass unit tolerance on parent and fragment ions. The search was limited to the *Mus musculus* taxonomy. Scaffold was used to validate MS/MS based peptide and protein identifications. Peptide identifications were accepted if they could be established at greater than 95.0% probability as specified by the Peptide Prophet algorithm (23). Protein identifications were accepted if they could be established at greater than 99.0% probability and contained at least 2 identified peptides. Protein probabilities were assigned by the Protein Prophet algorithm (24). Proteins that contained similar peptides and could not be differentiated based on MS/MS analysis alone were grouped to satisfy the principles of parsimony. These criterions limited our list to 880 proteins on top of which we add three proteins of interest that were identified by one peptide which sequences were manually validated (Flotillin-1, Beclin-1 and Regulator of G-protein signalling 19).

The false discovery rate (FDR) was determined according to Choi et al (25) false positive identification error method. With a protein probability of 99% and 1 peptide at 95%, the false discovery rate is 0.22% for the proteins and 0.0098% for peptides. For each of the 883 proteins in this final list, we assigned a consensus name and a functional category with the help of the public databases Uniprot (http://www.uniprot.org/uniprot/), Ensembl! (http://www.ensembl.org), GeneCard (http://www.genecards.org/), Gene Ontology (http://www.geneontology.org/), Expasy (http://us.expasy.org) and literature search. Data mining of the final list was conducted in a MySQL database using Navicat 8 (http://navicat.com/) as graphical user interface. The Venn diagram was generated using BioVenn (26).

Protein relative abundance was determined using a redundant peptide counting approach (27, 28). The average value of the redundant peptide counts (RPC) from the three identification cycles was determined at each time-point in fractions 1 and 7. The average RPC values were used to generate heat maps representing the abundance of the identified proteins at the different time-points, either in the total phagosome (average of fraction 1 and fraction 7) or specifically in DRMs (average in fraction 1). Heat maps were generated with MatLab (Mathworks). We limited the heat map analysis to the proteins fulfilling one of these criterions; a) proteins with average RPC values that decreased of at least 2 between 30/0 and 30/240 (decreasing cluster), b) proteins with an average RPC value at the 30/30 time-point is more than 2 and correspond to more than 66% of the values at the 30/0 and the 30/240 time-points (transient cluster), c) proteins with average RPC values that increased of at least 2 between 30/0 and 30/240 (increasing cluster) and d) all other proteins identified by an average RPC of 2 for the 3 time points (stable cluster). This selective method gave us a list of 386 proteins for the phagosome heat map and 150 for the DRMs. In order to test whether the peptide count profiles were reproducible within time-points and protein fractions (DSMs, DRMs), while being distinct among fractions, we examined the patterns of correlation of the peptide profiles (RPC across all proteins). We correlated the profiles of peptide counts of all of the 18 different protein samples with each other (non-parametric Spearman correlation coefficient, ρ). Distances derived from the correlation coefficient ($1- \rho$) were then used to generate a hierarchical tree by the complete aggregation method for hierarchical clustering (Figure 1D). All these analyses were performed in R (29).

Protein-protein interaction networks

To highlight potential protein-protein interactions, the 386 phagosomal proteins eligible for the heat map were submitted to STRING (Search Tool for the Retrieval of Interacting Genes/Proteins http://string.embl.de) version 8.2, using the mouse database (Jensen et al. 2009). The STRING analysis generated a network of 377 proteins involved in 1030 interactions with a minimal confidence score of 0.400. We also considered protein-protein interactions data from a recent experiment on the budding yeast *Saccharomyces cerevisiae*. We previously established a genome-wide map of the yeast protein interaction using a Protein-fragment Complementation Assay (PCA), with proteins endogenously tagged (30). We therefore examined whether the mouse proteins identified as being associated with the phagosome in this study had yeast orthologs that have been shown to interact by PCA. Using yeast-to-mouse orthologies obtained from Ensembl! (http://www.ensembl.org/), we retrieved 483 yeast orthologs out of the 883 phagosomal proteins. Converting this network back to mouse proteins gave us 62 proteins involved in 109 hypothetical protein-proteins interactions. Among these proteins, we kept only the ones included in the 386 heat map eligible list and we obtain a new network of 36 proteins having 44 connections. These data were used to generate a protein-protein interaction network map with Cytoscape 2.6.0 and the plugin Bisogenet (31, 32).

Comparative genomics analysis

To identify the evolutionary origin of MS identified rafts and non-rafts phagosome proteins, comparative genomics and paralogues analyses were applied as performed in (33) except that PhylomeDB version 8 (34) was used and involved 69 taxa (*Aedes aegypti, Anopheles*

gambiae, Apis mellifera, Arabidopsis thaliana, Batrachochytrium dendrobatidis, Bos taurus, Branchiostoma floridae, Caenorhabditis briggsae, Caenorhabditis elegans, Caenorhabditis remanei, Candida albicans, Candida glabrata, Canis familiaris, Chlamydomonas reinhardtii, Ciona intestinalis, Ciona savignyi, Cryptococcus neoformans, Cyanidioschyzon merolae, Danio rerio, Debaryomyces hansenii, Dictyostelium discoideum, Drosophila melanogaster, Echinops telfairi, Encephalitozoon cuniculi, Felis catus, Gallus gallus, Gasterosteus aculeatus, Giberella zeae, Kluyveromyces lactis, Loxodonta africana, Macaca mulatta, Monodelphis domestica, Mus musculus, Myotis lucifugus, Nematostella vectensis, Neurospora crassa, Ornithorhynchus anatinus, Oryzias latipes, Otolemur garnettii, Pan troglodytes, Phytophthora ramorum, Rattus norvegicus, Rhizopus oryzae, Saccharomyces cerevisiae, Schistosoma mansoni, Schizosaccharomyces pombe, Sorex araneus, Fugu rubripes, Tetraodon nigroviridis, Thalassiosira pseudonana, Trichoplax adhaerens, Xenopus tropicalis, Yarrowia lipolytica, Oryza sativa, Dasypus novemcinctus, Leishmania major, Plasmodium falciparum, Tetrahymena thermophila, Trypanosoma cruzi, Paramecium tetraurelia, Gillardia theta).

Results

Proteomics and bioinformatics approaches were used to carry out a large-scale characterization of the spatio-temporal changes occurring to proteins during phagolysosome biogenesis. We analyzed phagosomes at three different steps of maturation including early phagosomes (30 min of latex bead internalization), maturing phagosomes (30 min pulse of bead and 30 min chase), and phagolysosomes (30 min pulse and 240 min of chase). Western blot analyses were performed to assess the maturation of phagosomes within the three time points chosen for our study (Fig. 1A). As expected, the late endosomal/lysosomal markers LAMP1 and Flotillin-1 both increased during phagosome maturation (10), while the cell surface marker Na,K-ATPase α subunit and the NADPH oxidase gp91phox subunit both decreased with time (35). The proteins present in phagosomal membrane microdomains were separated into a Triton X-100-soluble fraction and a Triton X-100-resistant membrane fraction for each time point. This procedure led to the flotation of detergent resistant membranes (DRMs) in fractions 1 and 2 of an OptiPrep™ gradient (see Fig. 1B), as assessed by the enrichment of Flotillin-1 and the ganglioside GM1. In contrast, Rab5a and Lamp1, two known markers of phagosomes, were not enriched in these fractions and remained with the bulk of detergent soluble membranes (DSMs) at the bottom of the gradient in fraction 6 and 7 (Fig.1B).

To identify proteins associated with DRMs, the first fraction of the Optiprep™ gradient was analyzed by liquid-chromatography tandem mass spectrometry (LC-MS/MS), while fraction 7 was used to identify proteins associated with DSMs. To be included in the list of phagosomal proteins, a protein had to have a score of 99%, with at least 2 peptides having greater than 95.0%

of identification probability (determine by the Protein Prophet and Peptide Prophet algorithm respectively: see Materials and Methods). This approach ensured the selection of highly representative proteins for each sample. Based on these criteria, a total of 18735 peptides matching 883 proteins were identified (Suppl. Table I and II), with a false discovery rate lower than 0.3%. Of these, 427 proteins were found in DRMs at some point during phagosome maturation. Grouping of proteins based on their identification in the different phagosome preparations indicated that a majority of proteins are present in all time points studied (Fig. 1C). Measurement of the relative abundance of each phagosomal protein allowed us to determine at which time point and in what part of the membrane (DRMs versus DSMs) any protein reached its maximum abundance level during phagolysosome biogenesis. To measure the relative abundance of proteins, we favored a redundant peptide counting approach (27) used previously to assess maturation events along the biosynthetic pathway (28). This approach is well suited to compare a high number of conditions and/or samples in a high dynamic range (36). Redundant peptide counting compares the number of tryptic peptides detected in the mass spectrometer for any given protein in all of the samples. Thus, the presence of a protein in a given sample can be coupled with a value of its relative abundance and compared to the other samples. A correlation matrix (not shown) and a hierarchical clustering analysis of the 18 samples (Fig 1D) were used to assess the efficiency of the redundant peptide counting approach. The latter analysis, which groups samples according to their level of similarity, led to the efficient clustering of the phagosome preparations according to their time point and their position in the membrane (DRMs vs DSMs), highlighting the reproducibility and specificity of each condition studied. Furthermore, the validity of the peptide counting approach was highlighted by the fact that several known early and late markers of phagosome maturation were more abundant in the early or late phagosome time point respectively. For example, we observed increasing levels of

lysosomal markers, such as LAMP1, LAMP2, LIMP2, Niemann Pick type C2, prosaposin, and Rab7, over time (Suppl. Table II). These markers are indeed expected to be recruited to phagosomes during phagolysosome biogenesis (37). Several established lipid raft protein markers, such as Flotillin-1, Stomatin, the Src-family kinase Lyn, CD44, and heterotrimeric G proteins (38) were identified in fraction 1. Moreover Flotillin-1, Flotillin-2, and Stomatin were predominantly identified in DRMs at the 30/240 time-point, in agreement with previous results showing that the recruitment of Flotillin-1 to phagosomes occurs late during the maturation process, as shown by both Western blotting and immunofluorescence microscopy (10). These proteins were also present in azurophil granule DRMs where they might play a role in the maintenance of microdomain structure and/or signaling function (39).

Some of the proteins identified in our phagosome preparations are normally associated to other organelles, including the nucleus (histones, helicases, RNA binding proteins), mitochondria (Cytochrome c oxydase, F1-ATPase, NADH dehydrogenase), and ribosomes (ribosomal subunits). We have shown previously that phagosome isolated by flotation display low levels of contamination (40). The recent finding that phagosomes extensively interact with autophagosomes (41, 42) suggests that this type of interaction would bring a wide variety of proteins to the phagosome lumen for degradation. Interestingly, we observed that phagosomes isolated from cells displaying high levels of autophagic activity contained higher levels of the aforementioned types of proteins (unpublished observations).

The relative abundance values obtained with the spectral count analyses allowed us to generate "heat maps" highlighting four distinct temporal behaviours (Fig. 2, Suppl. Table 3 and 4). Proteins showing their peak of abundance at the 30/0, the 30/30, or the 30/240 time-point

were respectively grouped in the decreasing, transient, or increasing clusters. In addition, 15 proteins did not show significant variation during maturation and were classified as "stable". When considering the entire phagosome proteome, proteins appeared to be equally distributed between the decreasing (35%), transient (28%), and increasing clusters (33%) (Fig. 2A). In contrast, the phagosomal proteins associated with DRMs displayed important variations between the different temporal clusters, as only 5% of the proteins present in DRMs were maximal at the 30/0 time-point, while 28% were maximal at the 30/30 time-point, and 64% were maximal at the 30/240 time-point (Fig. 2B). These data provide the first indication that DRMs are either recruited and/or formed on the phagosome membrane during maturation, pointing out that membrane microdomains may specifically regulate some of the functional properties acquired during phagosome maturation. Fig. 3 shows the distribution of groups of proteins involved in key phagosomal functions based on their relative abundance (heat maps) during phagosome maturation.

Based on the heat maps data, we grouped proteins according to their functional properties as well as their relative abundance in DRMs and DSMs during maturation, and used the STRING database to determine the nature of their interacting partners (Fig. 4A, a larger version of this figure is presented in Suppl. Fig. 4 in order to identify each of the proteins and their interacting partners). The current representation clearly highlights that a very low proportion of the proteins identified on early phagosomes are preferentially distributed to DRMs. The proportion of proteins preferentially distributed to DRMs increases during phagosome maturation, indicating that specialized foci at the phagosome membrane are likely to play key roles in the functional properties of this organelle. Additional interactions among the network were highlighted (Fig. 4B) by considering protein-protein interaction data from a recent experiment on the budding

yeast *Saccharomcyes cerevisiae,* where we established a genome-wide map of the yeast protein-protein interactions using PCA with proteins endogenously tagged (30). These include, for example, interaction between the yeast vacuolar Ca2+ ATPase PMC1 and the vacuolar ATPase VMA13 corresponding to mouse orthologs ATP2B1 and V1-ATPase H. Another example is the interaction between ARC40, a subunit of the ARP2/3 complex, and the β subunit of the capping protein (CP) CAP2, which are orthologous to the Arp 2/3 subunit 2 and CapZ beta that are part of the ARP2/3 and Capping complex respectively (see Suppl. Table V for a complete list of protein-protein interactions). These interactions inferred by orthology with yeast proteins are represented with red edges in Fig. 4B.

Further annotation of the proteins present on DRMs, based on literature searches and data available in UniProt, provided valuable insights regarding the modulation of phagosome functional properties during phagolysosome biogenesis, and the significance of sub-compartimentation in this process. Functional subgroups of proteins which appear to be regulated by their assembly in membrane microdomains, including intracellular signalling proteins, transmembrane transporters, cytoskeleton components and the molecules involved in membrane fusion, are highlighted in Fig. 5. Altogether, these data allowed us to draw the first molecular model of phagosome maturation that considers the grouping of selected proteins in organized membrane microdomains (Suppl. Fig 2A, B and C). A possible link between the proteins present in DRMs and the alteration of phagosome functions by the intracellular parasite *Leishmania* is also presented in Supp. Fig. 3.

We performed comparative genomics analyses among 61 taxa to identify the origin of the

883 DSMs and DRMs mouse phagosome proteins identified by mass spectrometry, by using the curated gene phylogeny databases PhylomeDB (phylomeDB.org) and Treefam (treefam.org) (Figure 6, Suppl. Table VII). Our analyses indicate that the most ancient proteins of the mouse phagosome proteome present in organisms such as amoeba, that use phagocytosis for nutrition (phagotrophy), are equally distributed among DSMs and DRMs structures. In contrast, proteins that emerged in organisms where phagocytosis plays a key role in innate immunity (Bilateria to Chordata), as well as in adaptive immunity (Euteleostomi to mammals) are preferentially distributed to DRMs, suggesting that a complexification of these structures occurred during evolution (Fig. 6A). Classification of proteins according to their main functional properties highlighted the acquisition of sets of membrane receptors and signaling molecules by DRMs during evolution (Fig 6B). Remarkably, protein-protein interaction analyses revealed that although the DRMs proteins of ancient origin (phagotrophy) interact to a similar level with proteins present in DSMs or DRMs, those of more recent origin (innate and adaptive immunity) interact to a much higher level with proteins present in DRMs (Fig. 7A). For example, figure 7B shows that the protein network assembled around the small GTPase Rac1, emerging in phagotrophic organisms, is equally made of proteins present in DRMs (squares) and DSMs (circles). In contrast the complex network assembled around integrin proteins including ITGA4, ITGA5, ITGB1, ITGB2, and ITGAM, that appeared with innate immunity, is almost entirely built with proteins present in DRMs. Altogether, these data strongly suggest that DRMs were either not present or much simpler in ancient organisms.

It is well established that gene duplication plays an important role in the emergence of novel functional properties by allowing one of the gene copies to mutate or to be reorganized extensively (65). Indeed, duplication of genes (paralogs) has been shown to contribute to the

complexification of organelles during evolution (66, 67). Our phylogenetic analyses identified 269 pairs of paralogs from the phagosome proteins present in our proteomics data. These analyses further indicated that a significantly higher proportion of the paralogs pairs had the two proteins in DRMs (43.9%). In contrast, only 16.4% of the paralogs pairs had both members in DSMs (Fig 8A). Interestingly, distinct functional families of proteins were expanded in DRMs and DSMs (Fig. 8B). These data suggest that gene duplication contributed to the complexification of DRMs.

Discussion

Studying the biogenesis of membrane organelles is hampered by the limitation of the fractionation procedures used to isolate these cellular structures at various stages of their formation. Nevertheless, phagosomes are particularly well-suited for this type of study. Indeed these organelles can be formed *de novo* after the internalization of large particulate materials, such as latex particles, enabling their isolation on a single sucrose gradient at precise points during their biogenesis. Considering the key roles played by phagosomes in both innate and adaptive immunity (43), their thorough characterization is part of a strategy to gain unique insights into the molecular mechanisms regulating immune functions. The functional properties of phagosomes are acquired through a complex maturation process by which nascent phagosomes, formed at the cell surface, are transformed into phagolysosomes. Phagolysosome biogenesis has initially been described as a process occurring through time. Accordingly, different sets of proteins have been shown to associates with maturing phagosomes and assigned to early or late phagosomes (4, 5, 44). More detailed analyses using proteomics led to the identification of a large group of proteins on phagosomes from different species and model organisms (6, 7, 35, 40, 45-48), providing unique insights into the potential functions of this organelle. One of the novel concepts derived from these studies was that phagosomes display membrane microdomains where specific proteins assemble (7, 10, 14). This novel finding indicated that rather than being an organelle where lipids and proteins are randomly distributed, the phagosome membrane displays microdomains where specific molecules are segregated, enabling specialized functions to occur. Hence the regulation of phagosome functions during phagolysosome biogenesis would occur not only on a temporal basis, but also through changes in the profile of proteins present in specific regions of the organelle membrane. The data presented

here provide the first assessment of the complex modulation of the phagosome proteome occurring during phagolysosome biogenesis. Furthermore, the concomitant analysis of the detergent-soluble and -insoluble fractions of phagosomes provides the first thorough characterization of the dynamic reorganization of the phagosome membrane occurring during phagolysosome biogenesis.

Specific modifications of the phagosome composition during phagolysosome biogenesis have been described in previous studies, highlighting, for example, the acquisition of proteins linked to the ability of phagosomes to kill and degrade microorganisms for antigen presentation (37, 48, 49). As expected, our data indicate that phagolysosome biogenesis is accompanied by the acquisition of various hydrolases. Specifically, cathepsin B, D and Z increased throughout phagolysosome maturation, while cathepsin A, L and S reached their maximal level in intermediate phagosomes, suggesting that these enzymes are not transferred to phagosomes in bulk, but rather from different sources. Subunits of the proton pump V-ATPase involved in the acidification of the phagosome lumen and the activation of hydrolases also accumulate on maturing phagosomes. These results are consistent with a recent study where the abundance of proteins was measured by the incorporation of labelled amino acids (SILAC) (47). Some of the V-ATPase subunits may have an additional function during phagosome maturation. It has been proposed that the V0 domain plays a direct role in membrane fusion (50). The identification of *trans*-complexes between V0 domains in adjacent membranes showing the same dependence on inhibitors and activators as the fusion process itself led to the proposal that, after SNARE mediated docking, these *trans*complexes promote the mixing of the lipid bilayers by virtue of the highly hydrophobic proteolipid subunits (50). Interestingly, our results confirmed that the SNARE protein syntaxin 7 accumulates in late phagosomes (51), supporting the notion that this

enrichment occurs specifically in detergent-insoluble parts of the membrane. The role of the lipid environment as regulator of V-ATPase activity was addressed by Lafoucade and colleagues who concluded that the DRMs association increased the pump activity by promoting V1-V0 coupling (52). Their results also indicated that the V1/V0 ratio increased during endosome maturation. Our data indicate that the V1/V0 ratio also increases during phagosome maturation, as well as the enrichment of both complexes in lipid microdomains, suggesting that the pumping activity of the V-ATPase preferentially takes place in DRMs (Suppl. Table VI). Other membrane maintenance proteins were also identified, such as several members of the annexin family. Whereas annexin A3, A4 and A11 were only identified in soluble fraction of the phagosome, annexin A1, A2 and A5 were also found in DRMs. Annexin A2 was reported to be located in lipid rafts (53, 54), while annexin A11 (with A6 and A7) were found in azurophil granules of human neutrophils (39).

Remarkably, our data indicate that very few proteins are present in DRMs in early phagosomes. Those early DRM resident proteins could come from the plasma membrane microdomains. Most of the proteins present in phagosome DRMs are observed at later steps of maturation, suggesting that some of the phagosomal functional properties may be acquired through the arrangement of specialized membrane microdomains. In that context, DRMs could be either formed *de novo* on phagosomes, or acquired already assembled through fusion events with other organelles like endosomes and lysosomes (55, 56). Our results showing that sets of proteins present at high levels in DRMs of phagolysosomes are initially observed in soluble parts of the membrane suggest that functional microdomains could assemble by the reorganization of the phagosome membrane. This is the case for a group of SNARE proteins composed of Syntaxin 8, vti1b, vti1a, VAMP7 and VAMP4, known to interact during membrane fusion (57-59). All of these proteins reach a maximal level at 30/30 in DSMs but peak in DRMs at 30/240

(Suppl. Table II). In some cases, interacting proteins present in DRMs (e.g. Galectin-1, Moesin, Leukosialin, Basigin, SHP substrate 1 and Tm 9 superfamily 2 which form a signalling network with CD47) were subsequently detected in soluble parts of the phagosome membrane, suggesting that modulation and/or termination of protein activity might also occur through a dynamic spatial reorganization.

In addition to *Leishmania* and *Brucella* mentioned above, *Mycobacterium tuberculosis* also appears to inhibit the assembly of these structures shortly after its internalization (13, 14, 60). In the case of *Leishmania*, it was shown that this parasite alters several of the functional properties of phagosomes, including the ability of this organelle to fuse with late endosomes and lysosomes (61). The inhibition of membrane fusion requires that the parasite surface molecule lipophosphoglycan (LPG) be targeted to membrane rafts at the phagosomal membrane (12). LPG is also known to alter the generation of oxygen superoxides, and the integrity of the actin network surrounding phagosomes (62). Interestingly, our data indicate that proteins involved in all of these functions, including proteins of the fusion machinery (SNARE and Rab protein), the NADPH oxidase subunits p22phox and gp91phox, as well as proteins involved in actin remodelling (e.g. actin, cofilin 1, profiling 1, formin-like 1, CapZ α-1, actinin-α 4) are present on DRMs at some points during phagosome maturation (see Suppl. Fig. 3). Hence, it is conceivable that *Leishmania* could disrupt multiple functions at once simply by altering the integrity of membrane microdomains. Descoteaux and colleagues suggested that LPG may impair the phagosomal recruitment of a newly identified exocytocis regulator, Synaptotagmin (Syt) V (63). They showed that Syt V is normally recruited to GM1-containing microdomains, and that the

inhibition of this association by LPG prevents the normal maturation of phagosomes (acquisition of V-ATPase and Cathepsin D) (63).

Our data also allowed us to perform the first large-scale comparative genomics analyses of the evolution of membrane microdomains. By comparing the origin of the proteins observed in DRMs and DSMs, the occurrence of gene duplication, and the nature of their protein-protein interaction networks, we were able to highlight several key features that might have governed the assembly of microdomains during evolution. Our data clearly indicate that the phagosomal proteins that emerged during evolution (from bilateria to mammals, compared to the most ancient proteins present in phagotrophic organisms such as amoeba) were directed to DRM structures, suggesting that evolution favored the assembly of these structures. Remarkably, while protein of ancient origin present in DRMs interacted to similar levels with proteins present in DRMs or DSMs, the DRMs proteins that emerged in bilateria (organisms such as drosophila were phagocytosis plays a key role in innate immunity) preferentially interacted with proteins present in DRMs. These data also support the proposal that the organization of membrane microdomains might have been favored by events that occurred during evolution. The advent of sterols in biological membranes is, without a doubt, one of the most important steps in the evolution of DRM structures (64). A large diversity of sterol species is found among eucaryocytes. Ergosterol and phytosterols are mainly observed in yeast and plants membranes, whereas in mammalian cholesterol is the main membrane-active sterol. It is proposed that increasing atmospheric oxygen concentrations were the driving force behind the diversification of the structure of sterol molecules and their transformation into cholesterol (64-66). It is of interest to note that vertebrates, from fish to man, are the only animals that can synthesized cholesterol from sterol endogenously (65), a feature that may contribute to the ability of cells to assemble and modulate membrane microdomains on organelles. In that context, future analyses of the lipid

molecules present on phagosomes and how they are distributed within microdomains will be of high interest. However, this will require the development of novel methods that enable the isolation of membrane microdomains with detergents or chemicals compatible with mass spectrometry analyses.

Altogether, our proteomics analyses indicate that phagosome microdomains are dynamic structures that can assemble and disassemble during phagolysosome biogenesis. By doing so, they actively contribute to the modulation of phagosome functional properties. Key events linked with the emergence of novel proteins and duplication events, as well as changes in lipid composition, are likely to have contributed to the emergence of microdomains during evolution.

Acknowledgements

The authors wish to thank the Human Frontier Science Program (M.D.), the Canadian Institute for Health Research (CIHR) (M.D., S.W.M, P.T), and Génome-Québec for their support. C.R.L is a CIHR New Investigator. LBB is a scholar of the Fonds de la Recherche en Santé du Québec (FRSQ). We also wish to thank Christiane Rondeau, Annie Laplante, Line Roy, Marcos R. Di Falco and Simon Letarte for their assistance in generating the proteomics data.

References

1. Haas, A. (2007) The phagosome: compartment with a license to kill. *Traffic* 8, 311-330.
2. Jutras, I., Laplante, A., Boulais, J., Brunet, S., Thinakaran, G., and Desjardins, M. (2005) Gamma-secretase is a functional component of phagosomes. *J Biol Chem* 280, 36310-36317.
3. Vyas, J. M., Van der Veen, A. G., and Ploegh, H. L. (2008) The known unknowns of antigen processing and presentation. *Nat Rev Immunol* 8, 607-618.
4. Desjardins, M., Huber, L. A., Parton, R. G., and Griffiths, G. (1994) Biogenesis of phagolysosomes proceeds through a sequential series of interactions with the endocytic apparatus. *J Cell Biol* 124, 677-688.
5. Pitt, A., Mayorga, L. S., Stahl, P. D., and Schwartz, A. L. (1992) Alterations in the protein composition of maturing phagosomes. *J Clin Invest* 90, 1978-1983.
6. Gotthardt, D., Blancheteau, V., Bosserhoff, A., Ruppert, T., Delorenzi, M., and Soldati, T. (2006) Proteomics fingerprinting of phagosome maturation and evidence for the role of a Galpha during uptake. *Mol Cell Proteomics* 5, 2228-2243.
7. Garin, J., Diez, R., Kieffer, S., Dermine, J. F., Duclos, S., Gagnon, E., Sadoul, R., Rondeau, C., and Desjardins, M. (2001) The phagosome proteome: insight into phagosome functions. *J Cell Biol* 152, 165-180.
8. Houde, M., Bertholet, S., Gagnon, E., Brunet, S., Goyette, G., Laplante, A., Princiotta, M. F., Thibault, P., Sacks, D., and Desjardins, M. (2003) Phagosomes are competent organelles for antigen cross-presentation. *Nature* 425, 402-406.
9. Simons, K., and Ikonen, E. (1997) Functional rafts in cell membranes. *Nature* 387, 569-572.
10. Dermine, J. F., Duclos, S., Garin, J., St-Louis, F., Rea, S., Parton, R. G., and Desjardins, M. (2001) Flotillin-1-enriched lipid raft domains accumulate on maturing phagosomes. *J Biol Chem* 276, 18507-18512.
11. Vilhardt, F., and van Deurs, B. (2004) The phagocyte NADPH oxidase depends on cholesterol-enriched membrane microdomains for assembly. *Embo J* 23, 739-748.
12. Winberg, M. E., Holm, A., Sarndahl, E., Vinet, A. F., Descoteaux, A., Magnusson, K. E., Rasmusson, B., and Lerm, M. (2009) Leishmania donovani lipophosphoglycan inhibits phagosomal maturation via action on membrane rafts. *Microbes Infect* 11, 215-222.
13. Arellano-Reynoso, B., Lapaque, N., Salcedo, S., Briones, G., Ciocchini, A. E., Ugalde, R., Moreno, E., Moriyon, I., and Gorvel, J. P. (2005) Cyclic beta-1,2-glucan is a Brucella virulence factor required for intracellular survival. *Nat Immunol* 6, 618-625.
14. Dermine, J. F., Goyette, G., Houde, M., Turco, S. J., and Desjardins, M. (2005) Leishmania donovani lipophosphoglycan disrupts phagosome microdomains in J774 macrophages. *Cell Microbiol* 7, 1263-1270.
15. Lingwood, D., and Simons, K. (2010) Lipid rafts as a membrane-organizing principle. *Science* 327, 46-50.
16. Foster, L. J., De Hoog, C. L., and Mann, M. (2003) Unbiased quantitative proteomics of lipid rafts reveals high specificity for signaling factors. *Proc Natl Acad Sci U S A* 100, 5813-5818.
17. Mannova, P., Fang, R., Wang, H., Deng, B., McIntosh, M. W., Hanash, S. M., and Beretta, L. (2006) Modification of host lipid raft proteome upon hepatitis C virus replication. *Mol Cell Proteomics* 5, 2319-2325.

18. Yang, W., Di Vizio, D., Kirchner, M., Steen, H., and Freeman, M. R. (2010) Proteome scale characterization of human S-acylated proteins in lipid raft-enriched and non-raft membranes. *Mol Cell Proteomics* 9, 54-70.
19. Gagnon, E., Duclos, S., Rondeau, C., Chevet, E., Cameron, P. H., Steele-Mortimer, O., Paiement, J., Bergeron, J. J., and Desjardins, M. (2002) Endoplasmic reticulum-mediated phagocytosis is a mechanism of entry into macrophages. *Cell* 110, 119-131.
20. Wessel, D., and Flugge, U. I. (1984) A method for the quantitative recovery of protein in dilute solution in the presence of detergents and lipids. *Anal Biochem* 138, 141-143.
21. Hiebl-Dirschmied, C. M., Adolf, G. R., and Prohaska, R. (1991) Isolation and partial characterization of the human erythrocyte band 7 integral membrane protein. *Biochim Biophys Acta* 1065, 195-202.
22. Wasiak, S., Legendre-Guillemin, V., Puertollano, R., Blondeau, F., Girard, M., de Heuvel, E., Boismenu, D., Bell, A. W., Bonifacino, J. S., and McPherson, P. S. (2002) Enthoprotin: a novel clathrin-associated protein identified through subcellular proteomics. *J Cell Biol* 158, 855-862.
23. Keller, A., Nesvizhskii, A. I., Kolker, E., and Aebersold, R. (2002) Empirical statistical model to estimate the accuracy of peptide identifications made by MS/MS and database search. *Anal Chem* 74, 5383-5392.
24. Nesvizhskii, A. I., Keller, A., Kolker, E., and Aebersold, R. (2003) A statistical model for identifying proteins by tandem mass spectrometry. *Anal Chem* 75, 4646-4658.
25. Choi, H., and Nesvizhskii, A. I. (2008) Semisupervised model-based validation of peptide identifications in mass spectrometry-based proteomics. *J Proteome Res* 7, 254-265.
26. Hulsen, T., de Vlieg, J., and Alkema, W. (2008) BioVenn - a web application for the comparison and visualization of biological lists using area-proportional Venn diagrams. *BMC Genomics* 9, 488.
27. Blondeau, F., Ritter, B., Allaire, P. D., Wasiak, S., Girard, M., Hussain, N. K., Angers, A., Legendre-Guillemin, V., Roy, L., Boismenu, D., Kearney, R. E., Bell, A. W., Bergeron, J. J., and McPherson, P. S. (2004) Tandem MS analysis of brain clathrin-coated vesicles reveals their critical involvement in synaptic vesicle recycling. *Proc Natl Acad Sci U S A* 101, 3833-3838.
28. Gilchrist, A., Au, C. E., Hiding, J., Bell, A. W., Fernandez-Rodriguez, J., Lesimple, S., Nagaya, H., Roy, L., Gosline, S. J., Hallett, M., Paiement, J., Kearney, R. E., Nilsson, T., and Bergeron, J. J. (2006) Quantitative proteomics analysis of the secretory pathway. *Cell* 127, 1265-1281.
29. R-Team, R. D. C. (2009) R: A language and environment for statistical computing. In: Computing, R. F. f. S., ed., Vienna, Austria.
30. Tarassov, K., Messier, V., Landry, C. R., Radinovic, S., Serna Molina, M. M., Shames, I., Malitskaya, Y., Vogel, J., Bussey, H., and Michnick, S. W. (2008) An in vivo map of the yeast protein interactome. *Science* 320, 1465-1470.
31. Cline, M. S., Smoot, M., Cerami, E., Kuchinsky, A., Landys, N., Workman, C., Christmas, R., Avila-Campilo, I., Creech, M., Gross, B., Hanspers, K., Isserlin, R., Kelley, R., Killcoyne, S., Lotia, S., Maere, S., Morris, J., Ono, K., Pavlovic, V., Pico, A. R., Vailaya, A., Wang, P. L., Adler, A., Conklin, B. R., Hood, L., Kuiper, M., Sander, C., Schmulevich, I., Schwikowski, B., Warner, G. J., Ideker, T., and Bader, G. D. (2007) Integration of biological networks and gene expression data using Cytoscape. *Nat Protoc* 2, 2366-2382.
32. Martin, A., Ochagavia, M. E., Rabasa, L. C., Miranda, J., Fernandez-de-Cossio, J., and Bringas, R. (2010) BisoGenet: a new tool for gene network building, visualization and analysis. *BMC Bioinformatics* 11, 91.

33. Boulais, J., Trost, M., Landry, C. R., Dieckmann, R., Levy, E. D., Soldati, T., Michnick, S. W., Thibault, P., and Desjardins, M. (2010) Molecular characterization of the evolution of phagosomes. *Mol Syst Biol* 6, 423.
34. Huerta-Cepas, J., Capella-Gutierrez, S., Pryszcz, L. P., Denisov, I., Kormes, D., Marcet-Houben, M., and Gabaldon, T. (2011) PhylomeDB v3.0: an expanding repository of genome-wide collections of trees, alignments and phylogeny-based orthology and paralogy predictions. *Nucleic Acids Res* 39, D556-560.
35. Jutras, I., Houde, M., Currier, N., Boulais, J., Duclos, S., LaBoissiere, S., Bonneil, E., Kearney, P., Thibault, P., Paramithiotis, E., Hugo, P., and Desjardins, M. (2008) Modulation of the phagosome proteome by interferon-gamma. *Mol Cell Proteomics* 7, 697-715.
36. Bantscheff, M., Schirle, M., Sweetman, G., Rick, J., and Kuster, B. (2007) Quantitative mass spectrometry in proteomics: a critical review. *Anal Bioanal Chem* 389, 1017-1031.
37. Kinchen, J. M., and Ravichandran, K. S. (2008) Phagosome maturation: going through the acid test. *Nat Rev Mol Cell Biol* 9, 781-795.
38. Pike, L. J. (2008) The challenge of lipid rafts. *J Lipid Res*.
39. Feuk-Lagerstedt, E., Movitz, C., Pellme, S., Dahlgren, C., and Karlsson, A. (2007) Lipid raft proteome of the human neutrophil azurophil granule. *Proteomics* 7, 194-205.
40. Stuart, L. M., Boulais, J., Charriere, G. M., Hennessy, E. J., Brunet, S., Jutras, I., Goyette, G., Rondeau, C., Letarte, S., Huang, H., Ye, P., Morales, F., Kocks, C., Bader, J. S., Desjardins, M., and Ezekowitz, R. A. (2007) A systems biology analysis of the Drosophila phagosome. *Nature* 445, 95-101.
41. Shui, W., Sheu, L., Liu, J., Smart, B., Petzold, C. J., Hsieh, T. Y., Pitcher, A., Keasling, J. D., and Bertozzi, C. R. (2008) Membrane proteomics of phagosomes suggests a connection to autophagy. *Proc Natl Acad Sci U S A* 105, 16952-16957.
42. Sanjuan, M. A., Dillon, C. P., Tait, S. W., Moshiach, S., Dorsey, F., Connell, S., Komatsu, M., Tanaka, K., Cleveland, J. L., Withoff, S., and Green, D. R. (2007) Toll-like receptor signalling in macrophages links the autophagy pathway to phagocytosis. *Nature* 450, 1253-1257.
43. Jutras, I., and Desjardins, M. (2005) Phagocytosis: at the crossroads of innate and adaptive immunity. *Annu Rev Cell Dev Biol* 21, 511-527.
44. Desjardins, M., Celis, J. E., van Meer, G., Dieplinger, H., Jahraus, A., Griffiths, G., and Huber, L. A. (1994) Molecular characterization of phagosomes. *J Biol Chem* 269, 32194-32200.
45. Burlak, C., Whitney, A. R., Mead, D. J., Hackstadt, T., and Deleo, F. R. (2006) Maturation of human neutrophil phagosomes includes incorporation of molecular chaperones and endoplasmic reticulum quality control machinery. *Mol Cell Proteomics* 5, 620-634.
46. Okada, M., Huston, C. D., Mann, B. J., Petri, W. A., Jr., Kita, K., and Nozaki, T. (2005) Proteomic analysis of phagocytosis in the enteric protozoan parasite Entamoeba histolytica. *Eukaryot Cell* 4, 827-831.
47. Rogers, L. D., and Foster, L. J. (2007) The dynamic phagosomal proteome and the contribution of the endoplasmic reticulum. *Proc Natl Acad Sci U S A* 104, 18520-18525.
48. Trost, M., English, L., Lemieux, S., Courcelles, M., Desjardins, M., and Thibault, P. (2009) The phagosomal proteome in interferon-gamma-activated macrophages. *Immunity* 30, 143-154.
49. Ramachandra, L., Simmons, D., and Harding, C. V. (2009) MHC molecules and microbial antigen processing in phagosomes. *Curr Opin Immunol*.

50. Peters, C., Bayer, M. J., Buhler, S., Andersen, J. S., Mann, M., and Mayer, A. (2001) Trans-complex formation by proteolipid channels in the terminal phase of membrane fusion. *Nature* 409, 581-588.
51. Collins, R. F., Schreiber, A. D., Grinstein, S., and Trimble, W. S. (2002) Syntaxins 13 and 7 function at distinct steps during phagocytosis. *J Immunol* 169, 3250-3256.
52. Lafourcade, C., Sobo, K., Kieffer-Jaquinod, S., Garin, J., and van der Goot, F. G. (2008) Regulation of the V-ATPase along the endocytic pathway occurs through reversible subunit association and membrane localization. *PLoS ONE* 3, e2758.
53. Fatimathas, L., and Moss, S. E. (2010) Annexins as disease modifiers. *Histol Histopathol* 25, 527-532.
54. Gerke, V., Creutz, C. E., and Moss, S. E. (2005) Annexins: linking Ca2+ signalling to membrane dynamics. *Nat Rev Mol Cell Biol* 6, 449-461.
55. Kobayashi, T., Stang, E., Fang, K. S., de Moerloose, P., Parton, R. G., and Gruenberg, J. (1998) A lipid associated with the antiphospholipid syndrome regulates endosome structure and function. *Nature* 392, 193-197.
56. Taute, A., Watzig, K., Simons, B., Lohaus, C., Meyer, H., and Hasilik, A. (2002) Presence of detergent-resistant microdomains in lysosomal membranes. *Biochem Biophys Res Commun* 298, 5-9.
57. Antonin, W., Fasshauer, D., Becker, S., Jahn, R., and Schneider, T. R. (2002) Crystal structure of the endosomal SNARE complex reveals common structural principles of all SNAREs. *Nat Struct Biol* 9, 107-111.
58. Flowerdew, S. E., and Burgoyne, R. D. (2009) A VAMP7/Vti1a SNARE complex distinguishes a non-conventional traffic route to the cell surface used by KChIP1 and Kv4 potassium channels. *Biochem J* 418, 529-540.
59. Mallard, F., Tang, B. L., Galli, T., Tenza, D., Saint-Pol, A., Yue, X., Antony, C., Hong, W., Goud, B., and Johannes, L. (2002) Early/recycling endosomes-to-TGN transport involves two SNARE complexes and a Rab6 isoform. *J Cell Biol* 156, 653-664.
60. Welin, A., Winberg, M. E., Abdalla, H., Sarndahl, E., Rasmusson, B., Stendahl, O., and Lerm, M. (2008) Incorporation of Mycobacterium tuberculosis lipoarabinomannan into macrophage membrane rafts is a prerequisite for the phagosomal maturation block. *Infect Immun* 76, 2882-2887.
61. Desjardins, M., and Descoteaux, A. (1997) Inhibition of phagolysosomal biogenesis by the Leishmania lipophosphoglycan. *J Exp Med* 185, 2061-2068.
62. Lodge, R., and Descoteaux, A. (2008) Leishmania invasion and phagosome biogenesis. *Subcell Biochem* 47, 174-181.
63. Vinet, A. F., Fukuda, M., Turco, S. J., and Descoteaux, A. (2009) The Leishmania donovani lipophosphoglycan excludes the vesicular proton-ATPase from phagosomes by impairing the recruitment of synaptotagmin V. *PLoS Pathog* 5, e1000628.
64. Brown, A. J., and Galea, A. M. (2010) Cholesterol as an evolutionary response to living with oxygen. *Evolution; international journal of organic evolution* 64, 2179-2183.
65. Nes, W. R. N. a. W. D. (1980) *Lipids in evolution*, 1st Ed., Plenum Press.
66. Barenholz, Y. (2002) Cholesterol and other membrane active sterols: from membrane evolution to "rafts". *Progress in lipid research* 41, 1-5.

Figure legends

Figure 1. **Validation of the phagosome DRMs isolation and the redundant peptide count** (A) J774 macrophages were fed latex beads for 30 min and chased for the indicated periods prior to phagosome isolation. Phagosomes were isolated and Western blotting was performed to detect know markers of maturation. The late markers LAMP1 and flotillin-1 increased during phagolysosome biogenesis, while the early markers Na,K-ATPase a subunit and gp91phox decreased. (B) DRMs were extracted from purified late phagosomes (30/240) with 1% Triton X-100 and isolated on an Optiprep^{TM}-step gradient. Seven fractions were collected, as well as a total membrane (TM) fraction, for Western blotting with the indicated proteins. Slot-blotting was performed to detect ganglioside GM1, a well known marker of DRMs. Proteins associated with DRMs are enriched in fractions 1 and 2, as demonstrated by the presence of flotillin-1 and GM1. LAMP1 and rab5a are not enriched in fraction 1. (C) A Venn diagram shows the overall distribution of the phagosome proteins identified by MS/MS at the three time points studied. A redundant peptide count was performed to evaluate the relative abundance of the proteins present in each group (time point, and presence in DRMs or DSMs). A correlation matrix (not shown), and hierarchical clustering (D) indicate that replicates of the same condition are more similar to each other than they are to other samples.

Figure 2. **Spatiotemporal profiling of phagosome proteins**. The distribution of the 386 eligible phagosome proteins (A), and 150 eligible DRM proteins (B) is presented in "heat maps", highlighting their relative abundance in these fractions during phagolysosome biogenesis (30/0 to 30/240) (see Experimental Procedures for eligibility criterions). The colors representing the

abundance are derived of the average value of the redundant peptide counts (RPC) for each proteins (light green; 0, and a gradient from green; > 0, to yellow, to red; >15).

Figure 3. **Spatio-temporal profiling of phagosome functional groups of proteins**. (A) Heat maps as in Fig. 2 showing proteins grouped by functional categories. For each category, only a maximum of the 5 most abundant proteins of each temporal behavior (decrease, transient, increase) are shown, according to the RPC (or a maximum of 15 proteins by category).

Figure 4. **Dynamic remodeling of the phagosome membrane during maturation.** (A) A network of predicted protein-protein interactions between 726 phagosome proteins was generated using the STRING database (blue edges). Note that it is possible to use the pdf viewer zoom tool to see all details in the online version of this figure (Supplemental Fig. 4). (B) New potential mouse protein-protein interactions for 94 phagosomal proteins were discovered using data from a Protein-fragment Complementation Assay (PCA) screen in the yeast *S. cerevisiae* (red edges). For A and B, the proteins are drawn only in the time point where they reach their maximal level. The proteins located in the gray outer circle are the ones identified only in the DSMs fraction of the phagosome while the inner circle represent proteins found in DRMs. The orange elipse show the proteins having a stable expression during the phagosome maturation.

Figure 5. **Recruitment of functional partners in the phagosome DRMs.** The distribution of proteins, and their interactions, indicate that groups of proteins involved in specific functions (highlighted by various colors) associate with DRMs during phagolysosome biogenesis. For each time point (30/0, 30/30 and 30/240) the proteins reaching their maximal intensity are drawn with strong colors, the faint ones represent all the other present in the DRMs.

Figure 6. **Evolutionary origin of the phagosome DRMs and DSMs proteins.** (A) Comparative genomics analyses of DRMs and DSMs proteins among 61 taxa identified the evolutionary origin of each protein. Proteome relative abundance (in %) of the evolutionary origin of DRMs and DSMs proteome are reported through three major evolutionary groups: phagotrophy (Eukaryota, Amoebozoa, and Fungi), innate immunity (Bilateria, Coelomata, and Chordata), and adaptive immunity (Euteleostomi and beyond). DSMs proteome is green DRMs proteome is red. (B) DRMs and DSMs relative abundance of functional categories through three major evolutionary groups of proteins.

Figure 7. **Levels of protein-protein interactions of DRMs proteins with proteins present in DRMs or DSMs.** (A) Protein-protein interaction data of DSMs and DRMs proteins were extracted and analyzed in order to observe if the evolution of DRMs proteins interact to the same level with DSMs or DRMs proteins. DRMs/DSMs interaction ratio values above 1 indicate higher level of interactions of DRMs proteins with DRMs proteins, whereas DRMs/DSMs interaction ratio values under 1 indicate higher level of interactions of DRMs phagosome proteins with DSMs proteins. (B) Example of protein-protein interaction networks assembled around the small GTPase Rac1 and different integrins including ITGA4, ITGA5, ITGB1, ITGB2, and ITGAM. DRMs proteins are in squares and DSMs proteins are in circles. The three evolutionary groups are represented in green (phagotrophy), yellow (innate immunity) and red (adaptive immunity).

Figure 8. **Paralogues content analysis of DRMs and DSMs proteomes.** (A) Of the 269 pairs of duplicated genes encoding for mouse phagosomal DRMs and DSMs proteins, we report the

relative abundance of these pairs through three groups of paralogs pairs: DRMs-DRMs, DRMs-DSMs and DSMs-DSMs. (B) DRMs-DRMs and DSMs-DSMs relative abundance of functional categories.

Figure 1

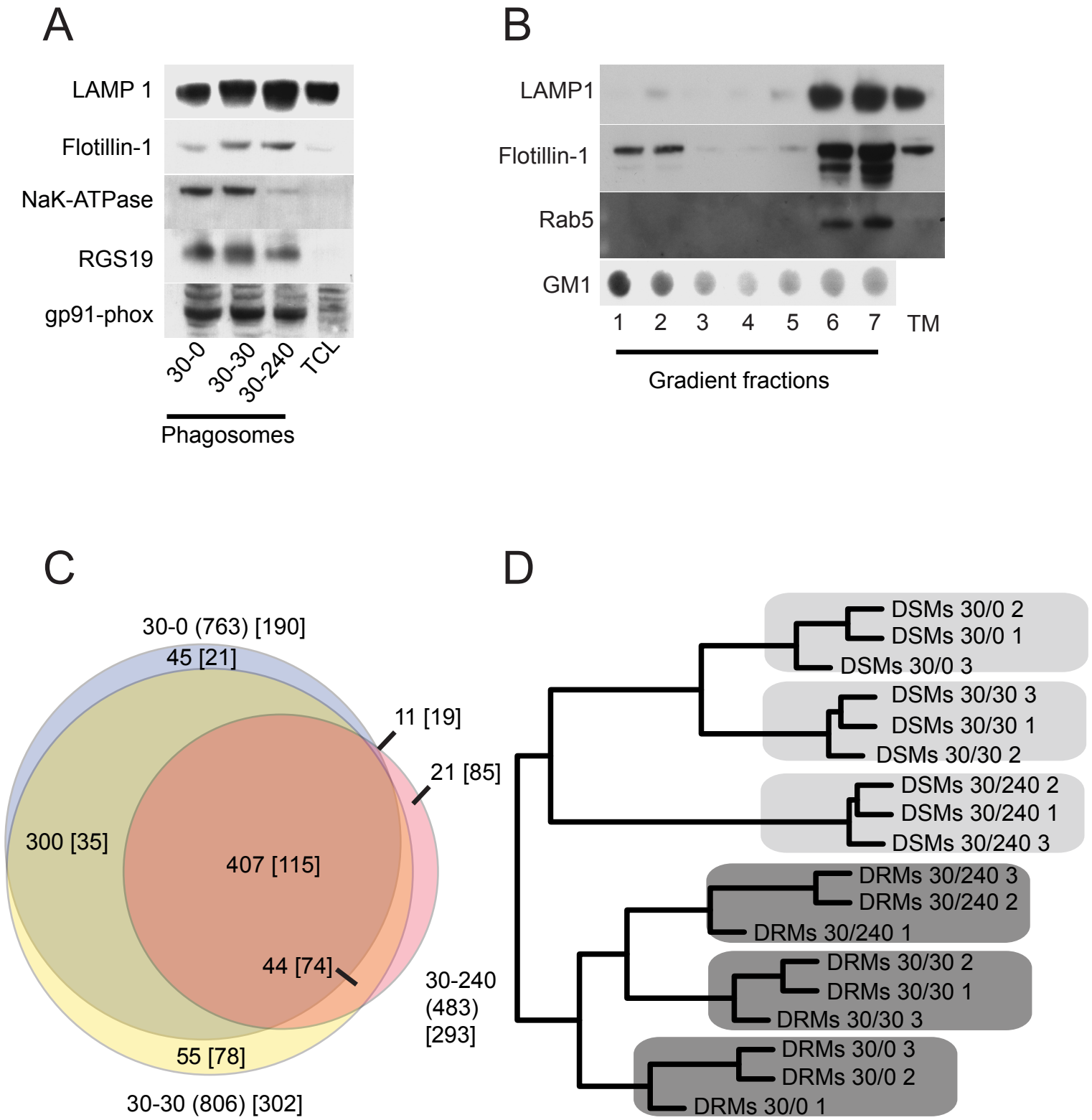
A
LAMP 1
Flotillin-1
NaK-ATPase
RGS19
gp91-phox
30-0
30-30
30-240
TCL
Phagosomes
B
LAMP1
Flotillin-1
Rab5
GM1
1
2
3
4
5
6
7
TM
Gradient fractions
C
30-0 (763) [190]
45 [21]
11 [19]
21 [85]
300 [35]
407 [115]
44 [74]
30-240
(483)
[293]
55 [78]
30-30 (806) [302]
D
DSMs 30/0 2
DSMs 30/0 1
DSMs 30/0 3
DSMs 30/30 3
DSMs 30/30 1
DSMs 30/30 2
DSMs 30/240 2
DSMs 30/240 1
DSMs 30/240 3
DRMs 30/240 3
DRMs 30/240 2
DRMs 30/240 1
DRMs 30/30 2
DRMs 30/30 1
DRMs 30/30 3
DRMs 30/0 3
DRMs 30/0 2
DRMs 30/0 1

Figure 2

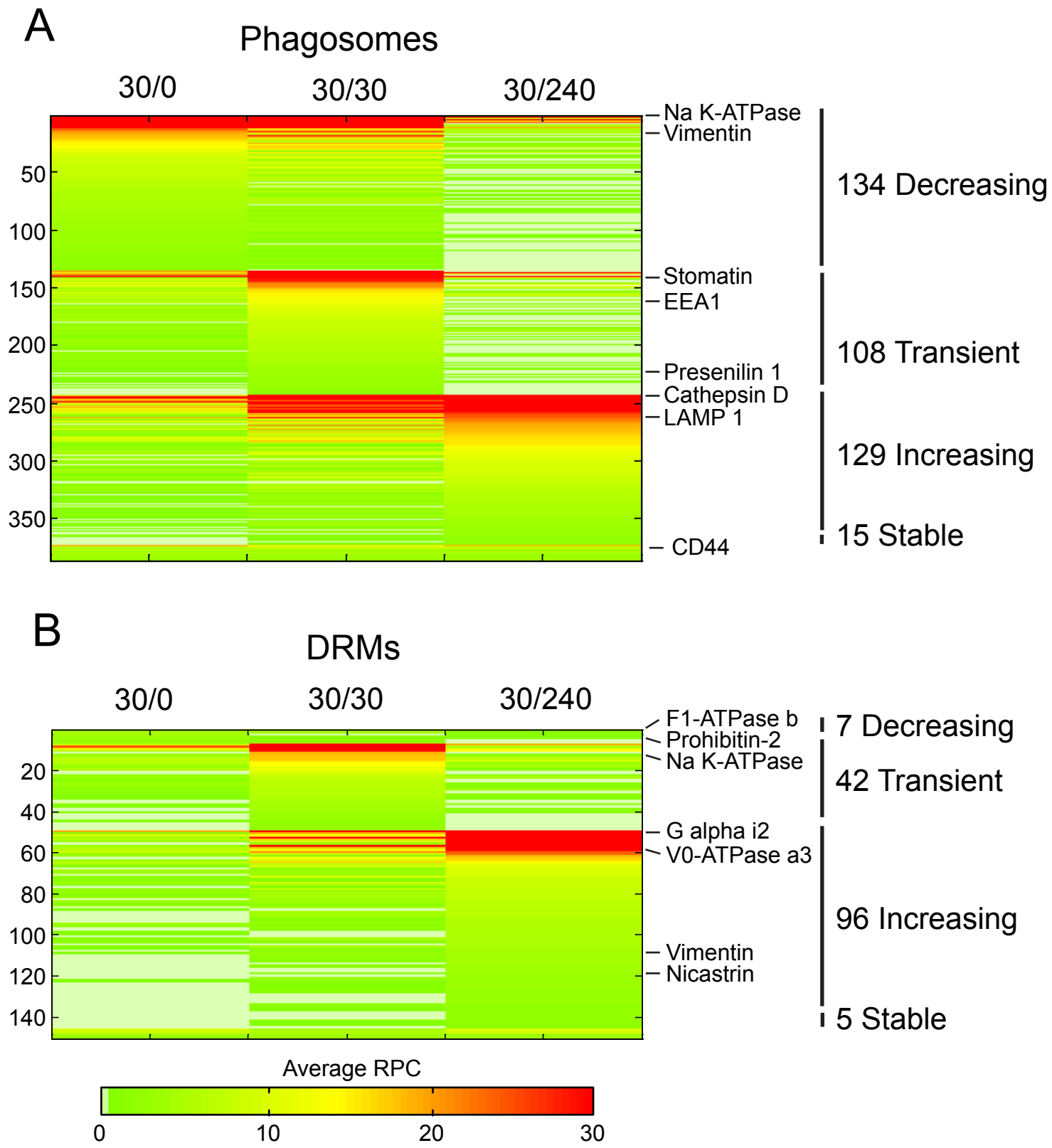
A
Phagosomes
30/0
30/30
30/240
50
100
150
200
250
300
350
Na K-ATPase
Vimentin
Stomatin
EEA1
Presenilin 1
Cathepsin D
LAMP 1
CD44
134 Decreasing
108 Transient
129 Increasing
15 Stable
B
DRMs
30/0
30/30
30/240
20
40
60
80
100
120
140
F1-ATPase b
Prohibitin-2
Na K-ATPase
G alpha i2
V0-ATPase a3
Vimentin
Nicastrin
7 Decreasing
42 Transient
96 Increasing
5 Stable
Average RPC
0
10
20
30

Figure 3

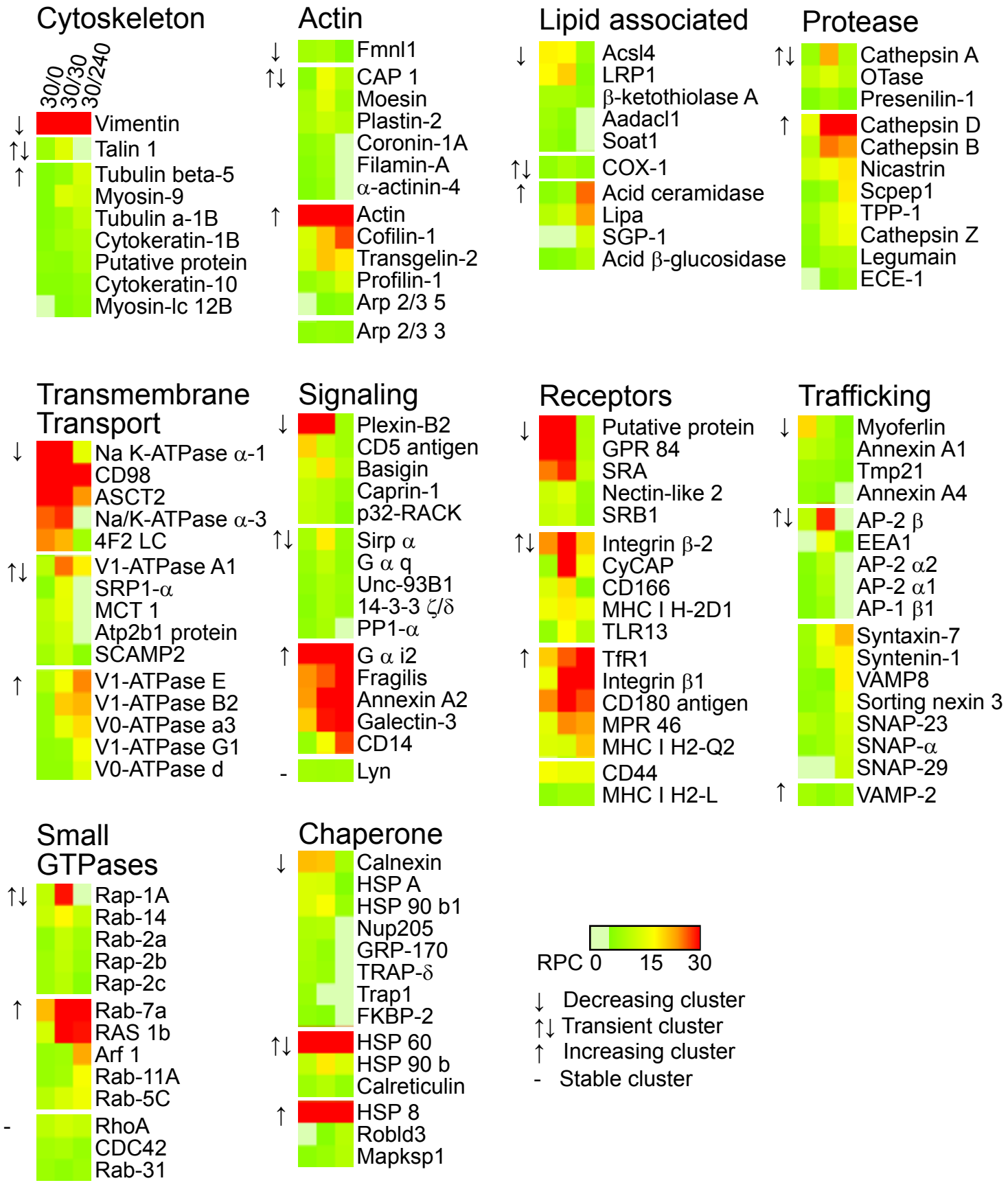
Cytoskeleton
30/0
30/30
30/240
↓ Vimentin
↑↓ Talin 1
↑ Tubulin beta-5
Myosin-9
Tubulin a-1B
Cytokeratin-1B
Putative protein
Cytokeratin-10
Myosin-lc 12B
Actin
↓ Fmnl1
↑↓ CAP 1
Moesin
Plastin-2
Coronin-1A
Filamin-A
α-actinin-4
↑ Actin
Cofilin-1
Transgelin-2
Profilin-1
Arp 2/3 5
Arp 2/3 3
Lipid associated
↓ Acsl4
LRP1
β-ketothiolase A
Aadacl1
Soat1
↑↓ COX-1
↑ Acid ceramidase
Lipa
SGP-1
Acid β-glucosidase
Protease
↑↓ Cathepsin A
OTase
Presenilin-1
↑ Cathepsin D
Cathepsin B
Nicastrin
Scpep1
TPP-1
Cathepsin Z
Legumain
ECE-1
Transmembrane Transport
↓ Na K-ATPase α-1
CD98
ASCT2
Na/K-ATPase α-3
4F2 LC
↑↓ V1-ATPase A1
SRP1-α
MCT 1
Atp2b1 protein
SCAMP2
↑ V1-ATPase E
V1-ATPase B2
V0-ATPase a3
V1-ATPase G1
V0-ATPase d
Signaling
↓ Plexin-B2
CD5 antigen
Basigin
Caprin-1
p32-RACK
↑↓ Sirp α
G α q
Unc-93B1
14-3-3 ζ/δ
PP1-α
↑ G α i2
Fragilis
Annexin A2
Galectin-3
CD14
- Lyn
Receptors
↓ Putative protein
GPR 84
SRA
Nectin-like 2
SRB1
↑↓ Integrin β-2
CyCAP
CD166
MHC I H-2D1
TLR13
↑ TfR1
Integrin β1
CD180 antigen
MPR 46
MHC I H2-Q2
CD44
MHC I H2-L
Trafficking
↓ Myoferlin
Annexin A1
Tmp21
Annexin A4
↑↓ AP-2 β
EEA1
AP-2 α2
AP-2 α1
AP-1 β1
Syntaxin-7
Syntenin-1
VAMP8
Sorting nexin 3
SNAP-23
SNAP-α
SNAP-29
↑ VAMP-2
Small GTPases
↑↓ Rap-1A
Rab-14
Rab-2a
Rap-2b
Rap-2c
↑ Rab-7a
RAS 1b
Arf 1
Rab-11A
Rab-5C
- RhoA
CDC42
Rab-31
Chaperone
↓ Calnexin
HSP A
HSP 90 b1
Nup205
GRP-170
TRAP-δ
Trap1
FKBP-2
↑↓ HSP 60
HSP 90 b
Calreticulin
↑ HSP 8
Robld3
Mapksp1
RPC 0 15 30
↓ Decreasing cluster
↑↓ Transient cluster
↑ Increasing cluster
- Stable cluster

Figure 4

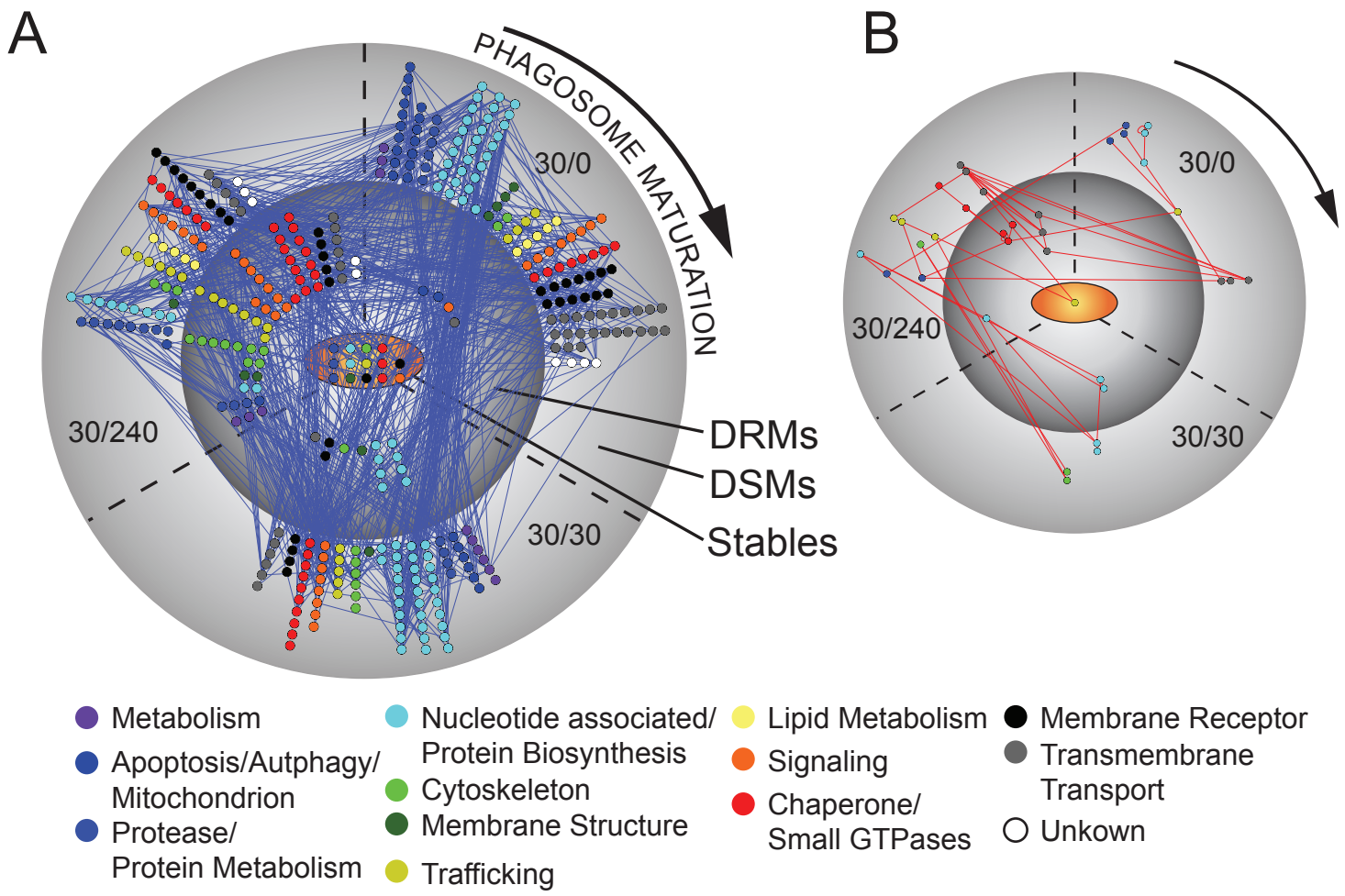
A
PHAGOSOME MATURATION
30/0
30/240
30/30
DRMs
DSMs
Stables
B
30/0
30/240
30/30
Metabolism
Apoptosis/Autphagy/ Mitochondrion
Protease/ Protein Metabolism
Nucleotide associated/ Protein Biosynthesis
Cytoskeleton
Membrane Structure
Trafficking
Lipid Metabolism
Signaling
Chaperone/ Small GTPases
Membrane Receptor
Transmembrane Transport
Unkown

Figure 5

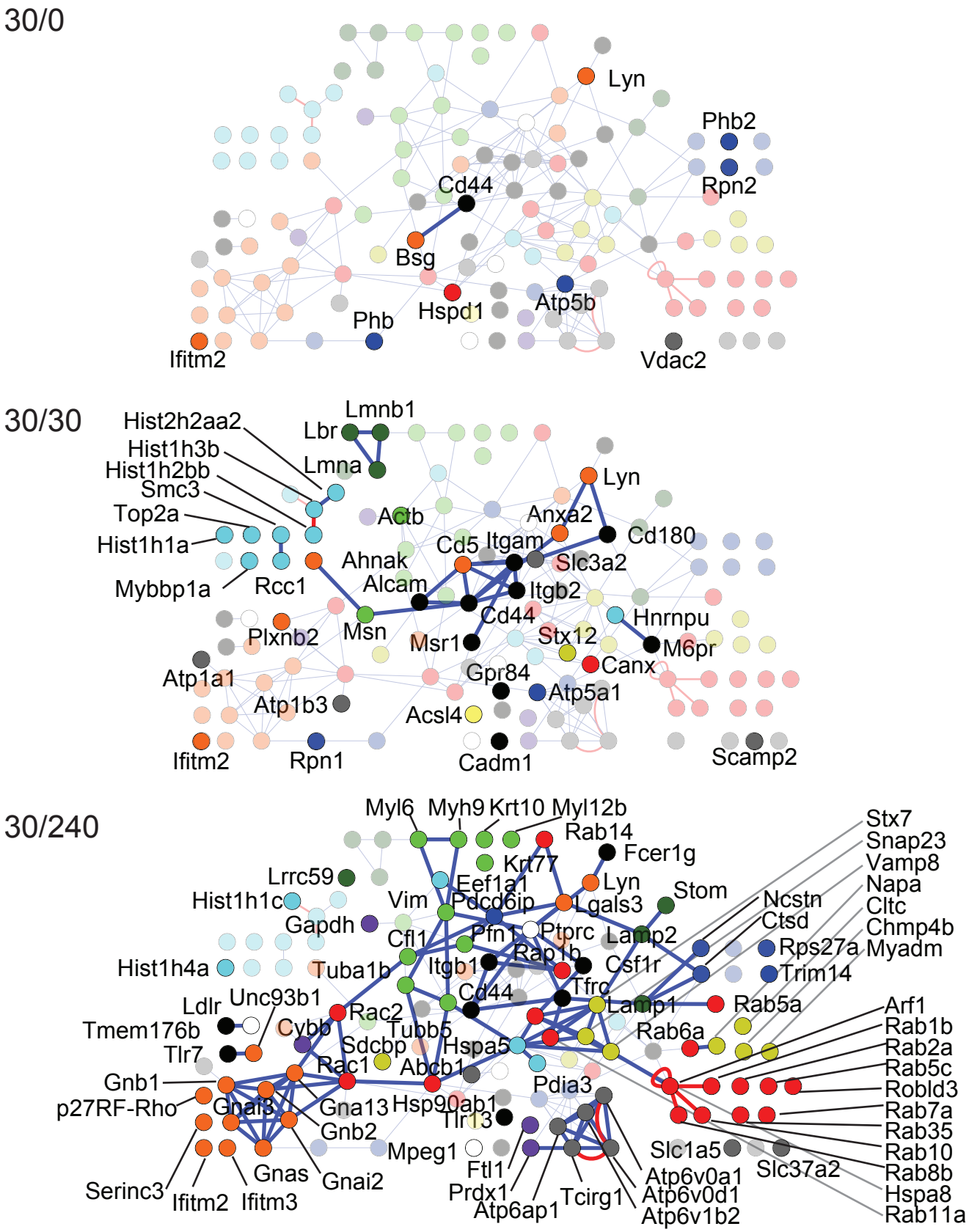
30/0
Lyn
Phb2
Rpn2
Cd44
Bsg
Hspd1
Atp5b
Phb
Ifitm2
Vdac2
30/30
Hist2h2aa2
Lmnb1
Lbr
Hist1h3b
Lmna
Hist1h2bb
Smc3
Top2a
Hist1h1a
Mybbp1a
Rcc1
Actb
Lyn
Anxa2
Cd180
Cd5
Itgam
Slc3a2
Ahnak
Alcam
Itgb2
Cd44
Hnrnpu
Plxnb2
Msn
Msr1
Stx12
M6pr
Canx
Atp1a1
Gpr84
Atp5a1
Atp1b3
Acsl4
Ifitm2
Rpn1
Cadm1
Scamp2
30/240
Myl6
Myh9
Krt10
Myl12b
Rab14
Fcer1g
Krt77
Lrrc59
Eef1a1
Lyn
Hist1h1c
Vim
Pdcd6ip
Lgals3
Stom
Gapdh
Cfl1
Pfn1
Ptprc
Lamp2
Hist1h4a
Tuba1b
Itgb1
Rap1b
Csf1r
Cd44
Tfrc
Ldlr
Unc93b1
Rac2
Lamp1
Rab5a
Tmem176b
Cybb
Tubb5
Rab6a
Tlr7
Sdcbp
Hspa5
Rac1
Abcb1
Gnb1
Pdia3
p27RF-Rho
Gnai3
Gna13
Hsp90ab1
Tlr13
Gnb2
Mpeg1
Slc1a5
Slc37a2
Serinc3
Gnas
Gnai2
Ftl1
Atp6v0a1
Ifitm2
Ifitm3
Prdx1
Tcirg1
Atp6v0d1
Atp6ap1
Atp6v1b2
Stx7
Snap23
Vamp8
Napa
Cltc
Chmp4b
Ncstn
Ctsd
Rps27a
Myadm
Trim14
Arf1
Rab1b
Rab2a
Rab5c
Robld3
Rab7a
Rab35
Rab10
Rab8b
Hspa8
Rab11a
Metabolism
Apoptosis/Autphagy/ Mitochondrion
Protease/ Protein Metabolism
Nucleotide associated/ Protein Biosynthesis
Cytoskeleton
Membrane Structure
Trafficking
Lipid Metabolism
Signaling
Chaperone/ Small GTPases
Membrane Receptor
Transmembrane Transport
Unkown

Figure 6

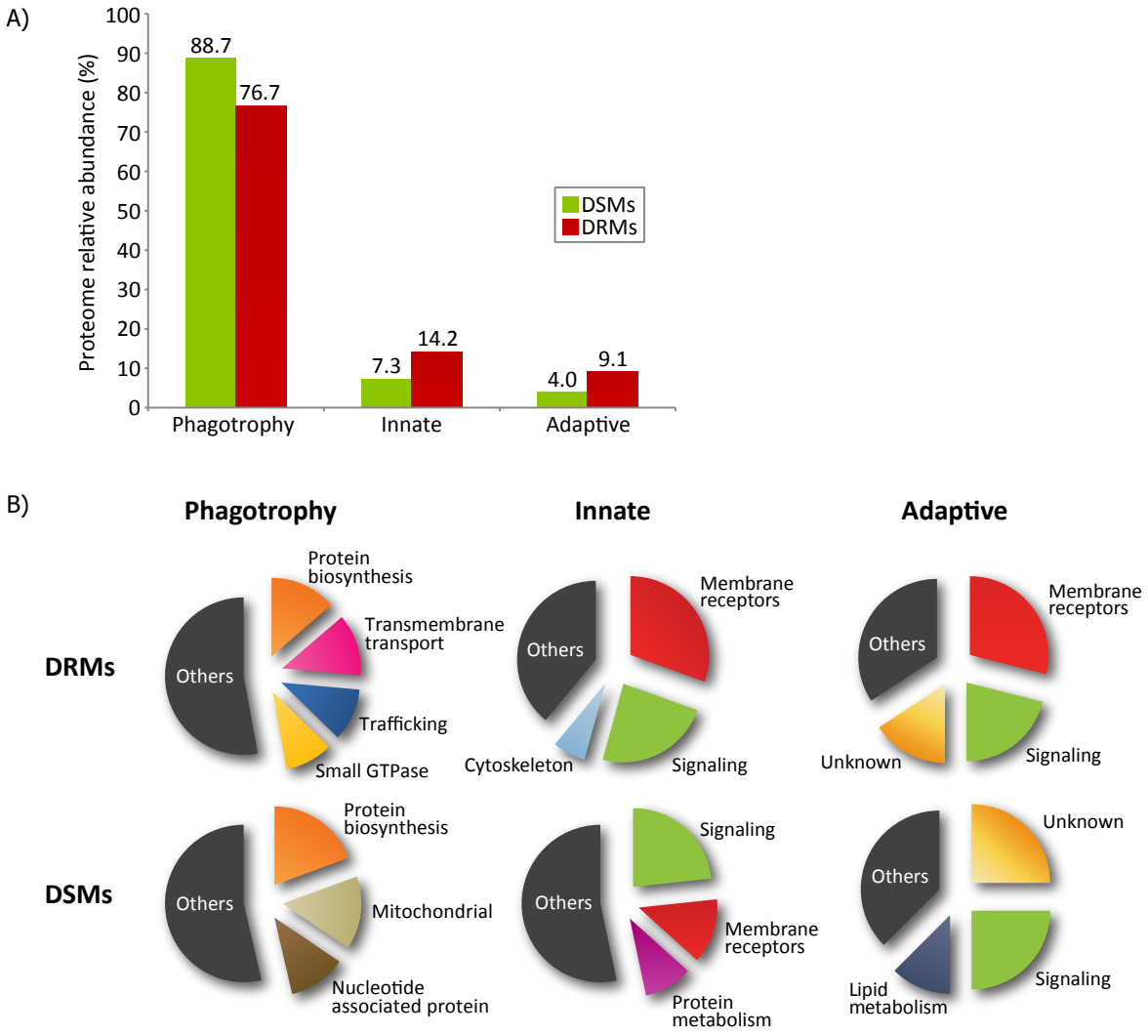
A)
Proteome relative abundance (%)
100
90
80
70
60
50
40
30
20
10
0
88.7
76.7
7.3
14.2
4.0
9.1
DSMs
DRMs
Phagotrophy
Innate
Adaptive
B)
Phagotrophy
Innate
Adaptive
DRMs
DSMs
Protein biosynthesis
Transmembrane transport
Others
Trafficking
Small GTPase
Membrane receptors
Others
Cytoskeleton
Signaling
Membrane receptors
Others
Unknown
Signaling
Protein biosynthesis
Others
Mitochondrial
Nucleotide associated protein
Signaling
Others
Membrane receptors
Protein metabolism
Unknown
Others
Lipid metabolism
Signaling

Figure 7

A)

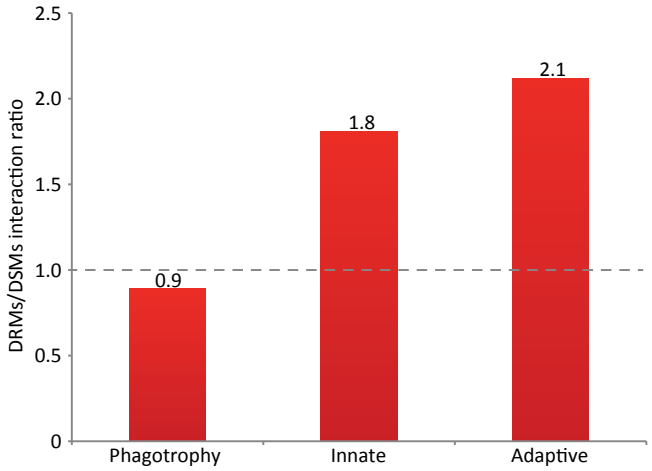
DRMs/DSMs interaction ratio
2.5
2.0
1.5
1.0
0.5
0
0.9
1.8
2.1
Phagotrophy
Innate
Adaptive

B)

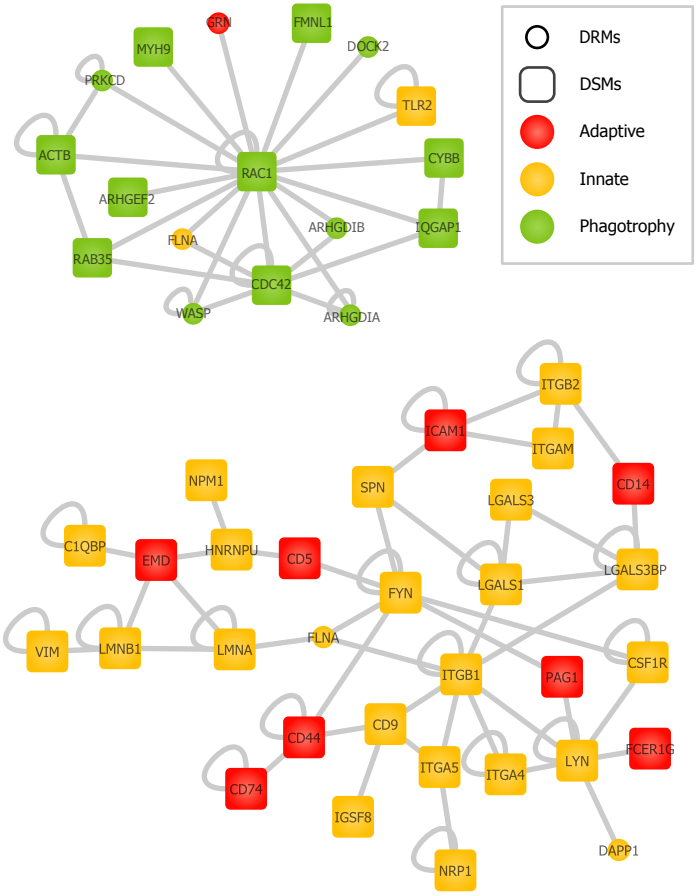
DRMs
DSMs
Adaptive
Innate
Phagotrophy
GRN
FMNL1
MYH9
DOCK2
PRKCD
TLR2
ACTB
RAC1
CYBB
ARHGEF2
ARHGDIB
IQGAP1
FLNA
RAB35
CDC42
WASP
ARHGDIA
ITGB2
ICAM1
ITGAM
NPM1
SPN
CD14
LGALS3
C1QBP
EMD
HNRNPU
CD5
LGALS3BP
FYN
LGALS1
VIM
LMNB1
LMNA
FLNA
CSF1R
ITGB1
PAG1
CD9
CD44
FCER1G
ITGA5
ITGA4
LYN
CD74
IGSF8
DAPP1
NRP1

Figure 8

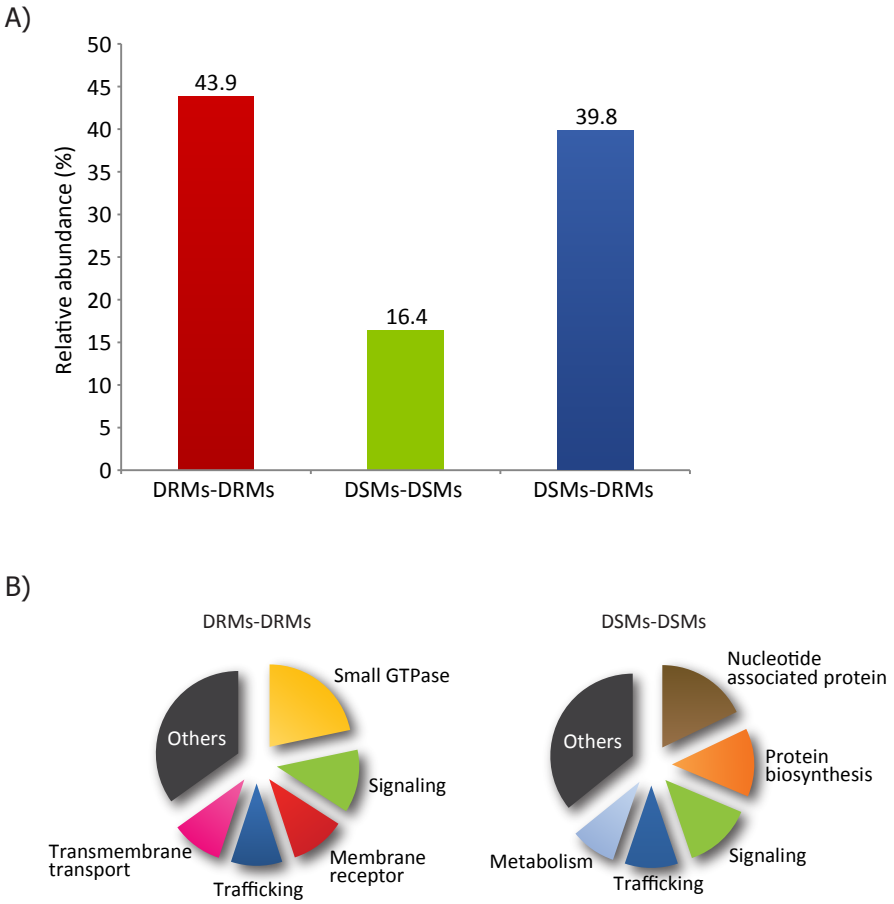
A)
Relative abundance (%)
50
45
40
35
30
25
20
15
10
5
0
43.9
16.4
39.8
DRMs-DRMs
DSMs-DSMs
DSMs-DRMs
B)
DRMs-DRMs
Small GTPase
Signaling
Membrane receptor
Trafficking
Transmembrane transport
Others
DSMs-DSMs
Nucleotide associated protein
Protein biosynthesis
Signaling
Trafficking
Metabolism
Others